Supporting Information – Word File

A novel aza-Paternò-Büchi reaction allows pinpointing carbon-carbon double bonds in unsaturated lipids by higher collisional dissociation

Andrea Cerrato, Anna Laura Capriotti*, Chiara Cavaliere, Carmela Maria Montone, Susy Piovesana, Aldo Laganà

Department of Chemistry, Sapienza University of Rome, Piazzale Aldo Moro 5, 00185 Rome, Italy

Table of Contents

Figure S11. ESI(–)-HCD MS/MS spectrum (30 NCE) of a) underivatized PI (18:1/18:1); b) aPB derivative of PI (18:1/18:1); c) PB derivative of PI (18:1/18:1).

Figure S12. Total ion current of a) deprotonated underivatized PI (18:1/18:1); b) deprotonated aPB derivative of PI (18:1/18:1); c) deprotonated PB derivative of PI (18:1/18:1) obtained by the competitive aPB/PB reaction.

Figure S13. ESI(–)-MS/MS spectrum (30 NCE) in negative ion mode of a) underivatized deprotonated PE (18:1/18:1); b) underivatized acetate adduct of PC (18:1/18:1).

Figure S14. Total ion current of the *m/z* corresponding to a) the deprotonated PB derivative of PC (16:0/18:1); b) the demethylated PB derivative of PC (16:0/18:1); c) acetate adduct of the PB derivative of PC (16:0/18:1); d) the protonated PB derivative of PC (16:0/18:1); e) the deprotonated aPB derivative of PC (16:0/18:1).

Figure S15. ESI(+)-HCD MS/MS spectrum (30 NCE) of (a) protonated underivatized PC (16:0/18:1) and (b) protonated PB-derivatized PC (16:0/18:1).

Figure S16. ESI(+)-HCD MS/MS spectrum (30 NCE) of protonated PB-derivatized PC (16:1/16:1) from the yeast extract. A zoom on the high m/z range shows a low abundance of the typical diagnostic peaks for pinpointing carbon-carbon double bonds.

Figure S17. ESI(–)-HCD MS/MS spectrum (30 NCE) in negative ion mode of a) underivatized acetate adduct of standard PC (16:0/18:1); b) deprotonated aPB derivative of standard PC (16:0/18:1).

Figure S18. Total ion current of the *m/z* corresponding to a) the protonated in-source fragment of the aPB derivative of FA 18:1 Δ9; b) the protonated in-source fragment of the aPB derivative of FA 18:1 Δ11; c) the deprotonated aPB derivative of FA 18:1 Δ9; d) the deprotonated aPB derivative of FA 18:1 Δ11.

Figure S19. ESI(+)-HCD MS/MS spectrum (30 NCE) of a) the protonated aPB derivative of FA 18:1 Δ9; b) the protonated aPB derivative of FA 18:1 Δ11. The diagnostic ions are marked with a red circle.

Figure S20. ESI(+)-HCD MS/MS spectrum (30 NCE) of a) the protonated aPB derivative of standard PI (18:1 Δ9/18:1 Δ9); b) the protonated aPB derivative of PE (18:1/18:1); c) the protonatedaPB derivative of PC (18:1/18:1). The diagnostic ions are marked with a red circle.

Table S1. Detailed LipidSearch parameters for polar lipids data processing.

Instrument	HCD
Peak Detection	
Recalc isotope	on
R.T. interval (min)	0.01
Search Options	
ExpType	LC-MS
Parent tol.	0.1 Da
NL/Prec tol.	0.5 Da
Precursor tol.	5.0 ppm
Product tol.	8.0 ppm
Merge Range (min.)	2.0
Min Peak Width (min.)	0.0
Intensity threshold	0.01 parent ion, threshold type: relative 1.0 product ion
m-Score threshold	2.0
Compound Rt Correction	
m/z tolerance	0.005 amu + 0.00 ppm
Warping based RT correction	Activated
Within batch Rt tolerance	0.1 min
Between batch Rt tolerance	0.2 min
Rt window	1 min
Target class	
Phospholipids	Lysophosphatidic acid, phosphatidic acid, lysophosphatidylcholine, phosphatidylcholine, lysophosphatidylethanolamine, phosphatidylethanolamine, lysophopshatidylglycerol, phosphatidylglycerol, lysophosphatidylinositol, phosphatidylinositol, lysophosphatidylserine, phosphatidylserine
Sphingolipids	Ceramides, glucosylsphingosine, lysosphingomyelin, sphingomyelin
Adducts	
negative	-H, +HCOO, +CH_3COO, -2H, -CH_3

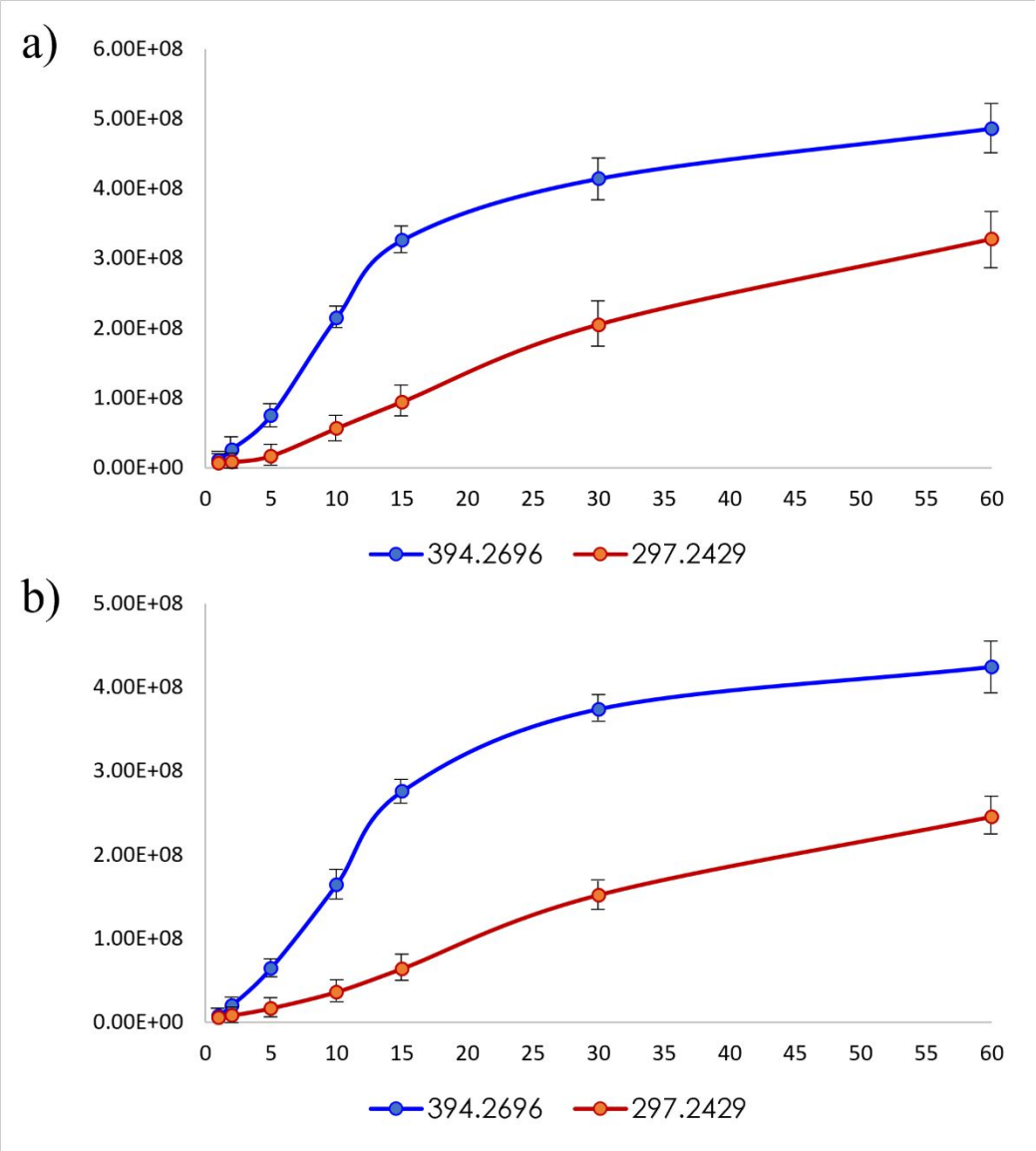

Figure S1. Dispersion graphs for FA 18:1 Δ9 (a) and FA 18:1 Δ11 (b) showing the total peak areas of *m/z* 394.2696 (6-AU derivative) and *m/z* 297.2429 (oxidized FA 18:1).

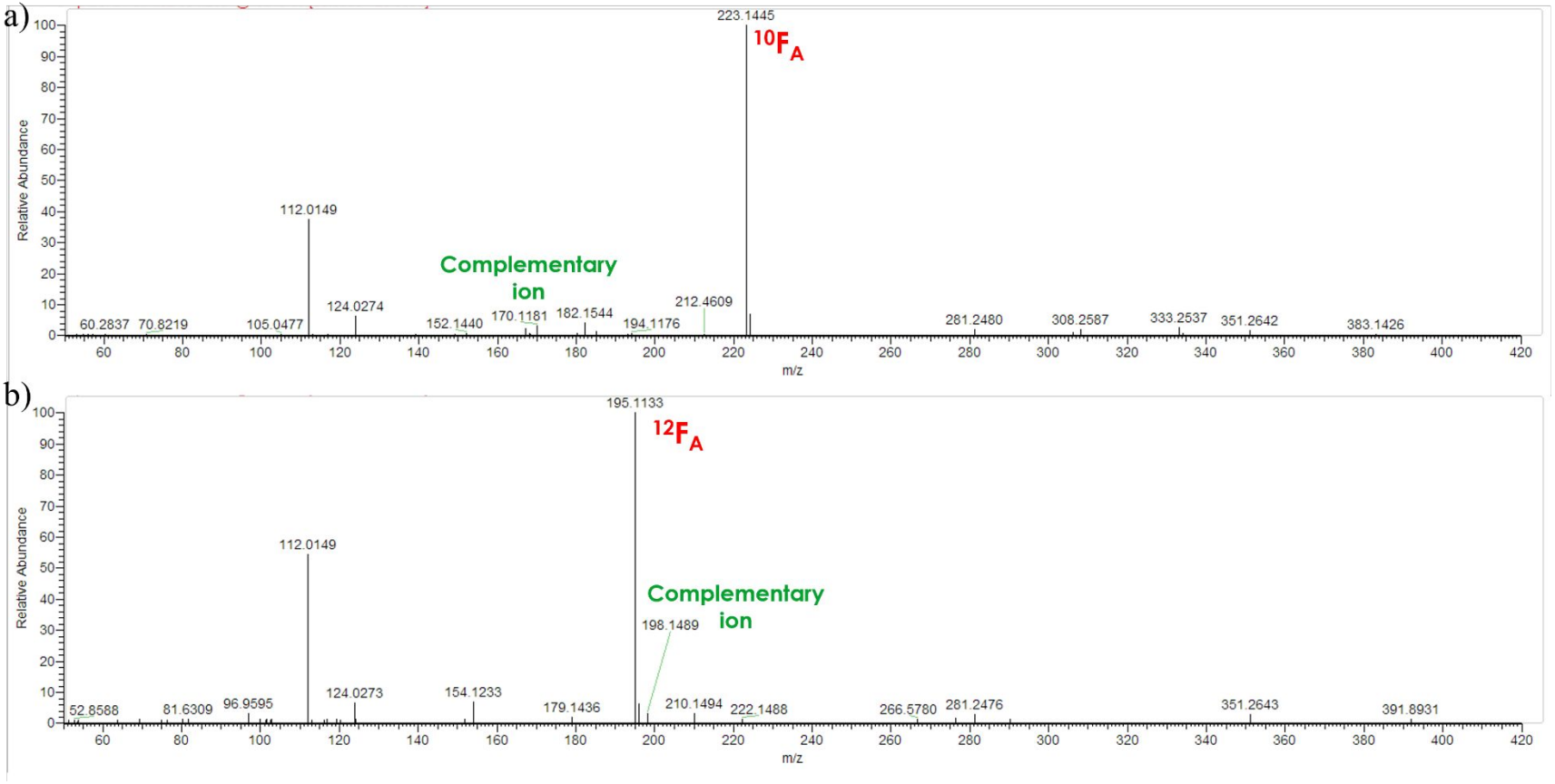

Figure S2. MS/MS scan associated to the aPB derivative P_A of FA 18:1 Δ9 (a) and FA 18:1 Δ11 (b). Other than the main F_A ion (base peak), the complementary ion is visible in the spectrum (m/z 170.1181 for 18:1 Δ9 and m/z 198.1489 for 18:1 Δ11)

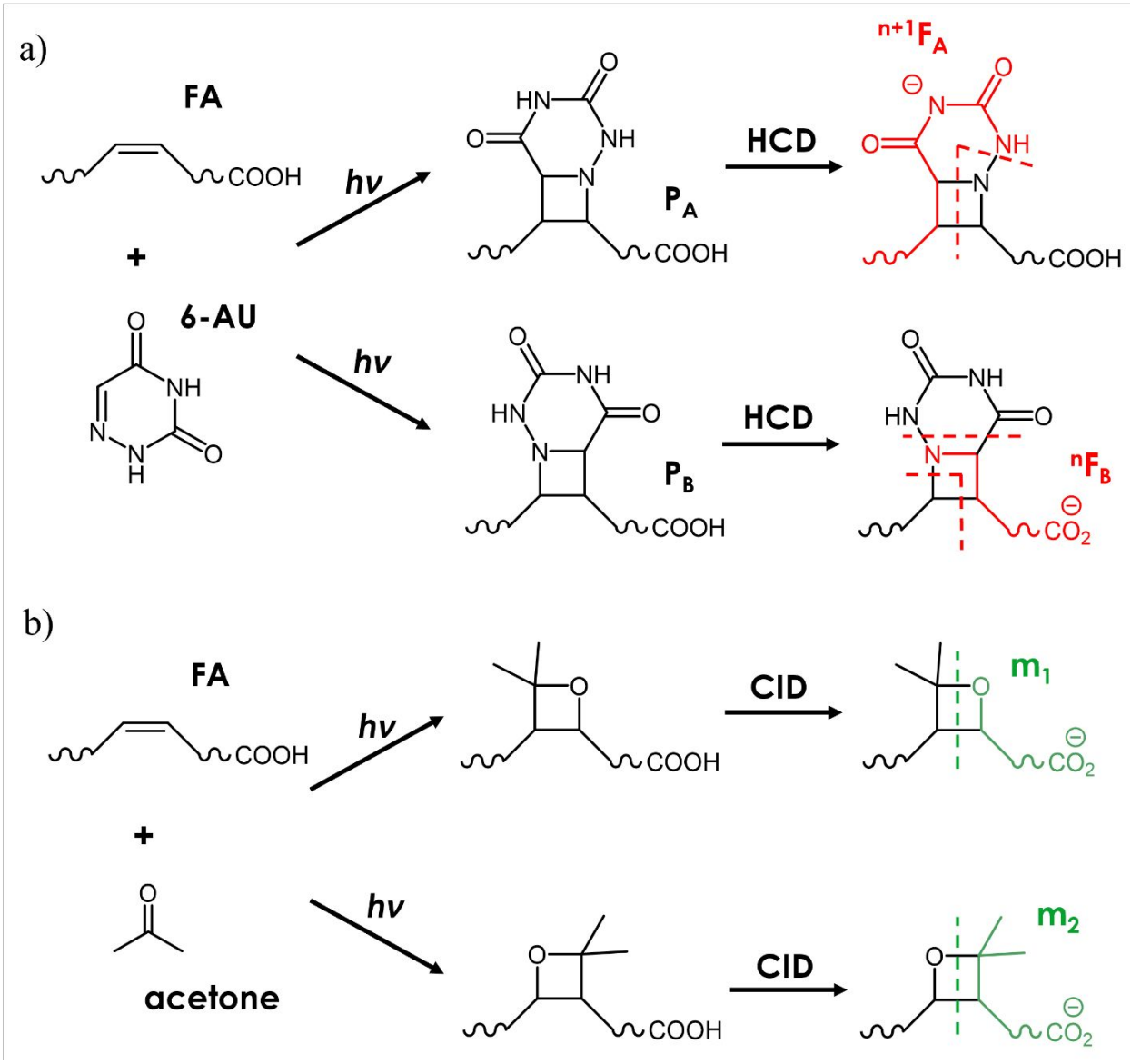

Figure S3. Comparison of the fragmentation pathways that lead to the diagnostic product ions between aPB reaction with 6-AU (a) and PB reaction with acetone (b).

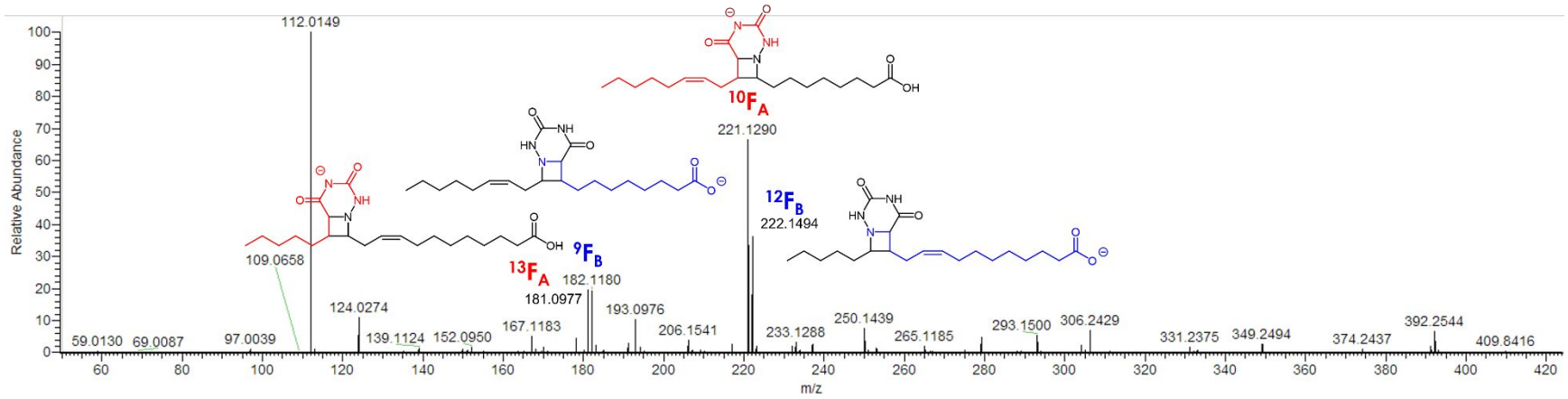

Figure S4. ESI(−)-HCD MS/MS spectrum (40 NCE) of deprotonated FA 18:2 Δ9,12 after photochemical reaction with 6-AU.

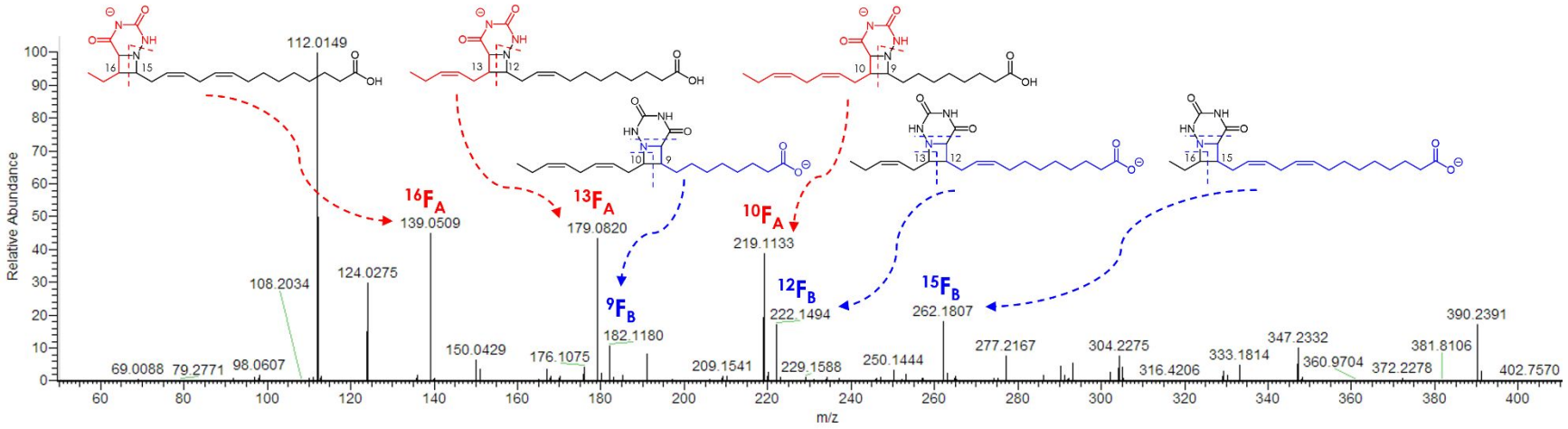

Figure S5. ESI(–)-HCD MS/MS spectrum (40 NCE) of deprotonated FA 18:3 Δ9,12,15 after photochemical reaction with 6-AU.

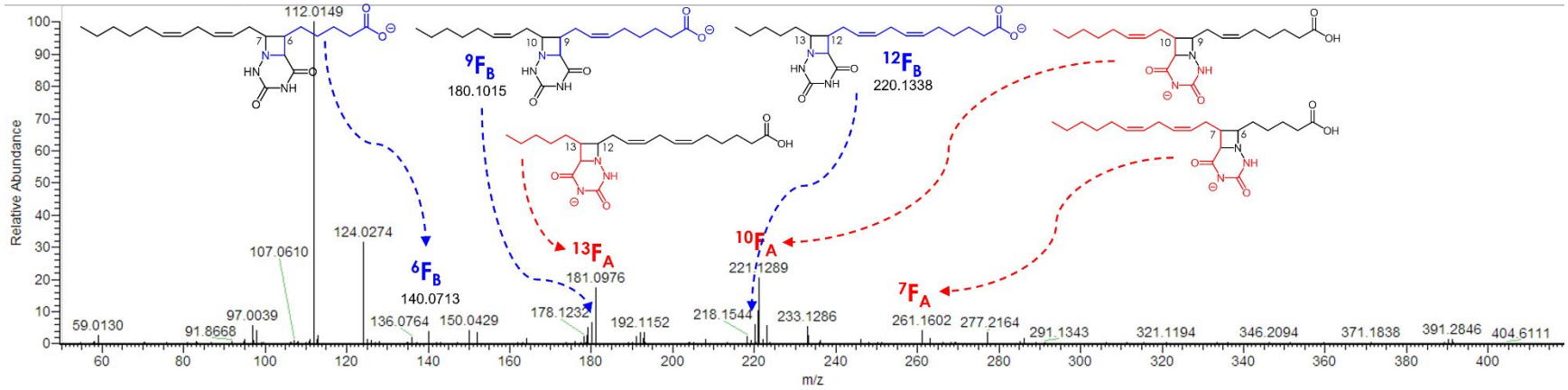

Figure S6. ESI(−)-HCD MS/MS spectrum (40 NCE) of deprotonated FA 18:3 Δ6,9,12 after photochemical reaction with 6-AU.

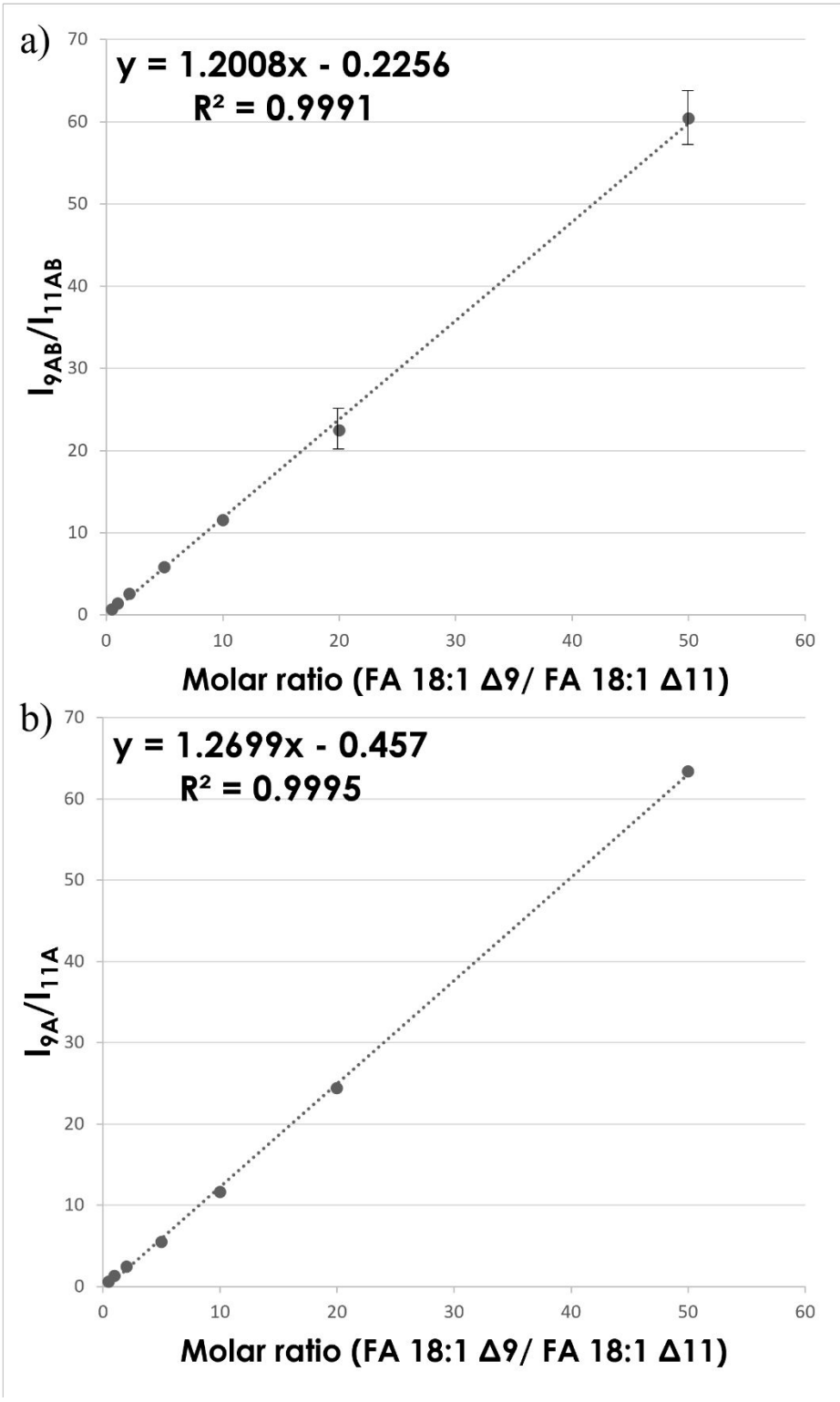

Figure S7. Linear relationship between the molar ratios of FA 18:1 Δ9 and Δ11 and: (a) the intensities of the diagnostic ion pairs (I_{9AB}/I_{11AB}), (b) the intensities of the diagnostic F_A ions (I_{9A}/I_{11A}).

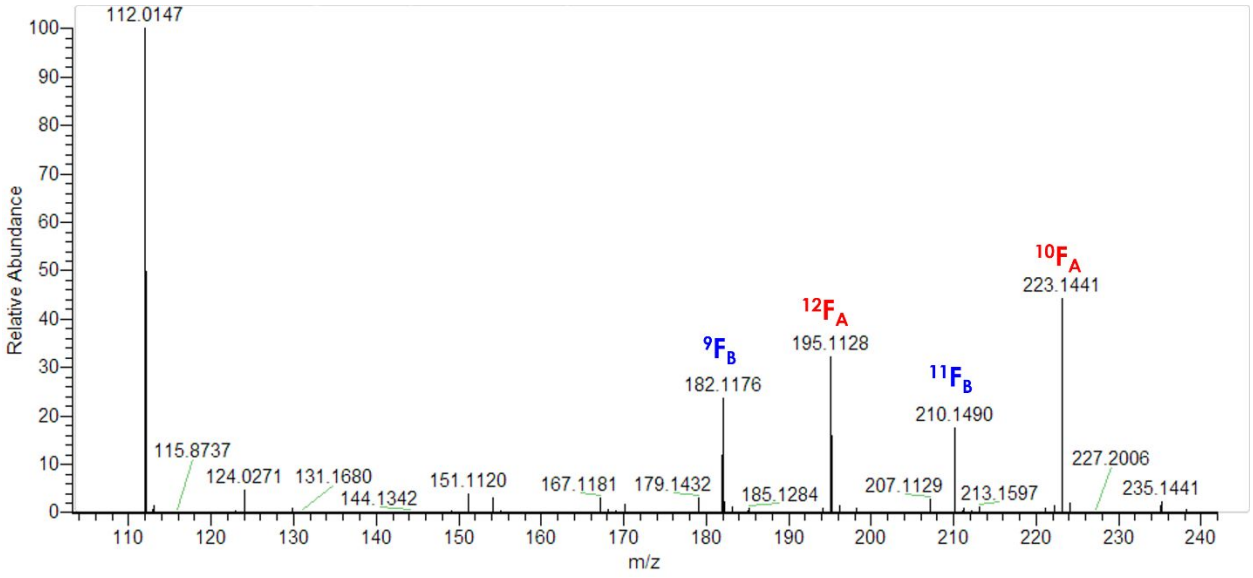

Figure S8. ESI(−)-HCD MS/MS spectrum (40 NCE) of FA 18:1 Δ9 and Δ11 at equal molar ratio after aPB derivatization.

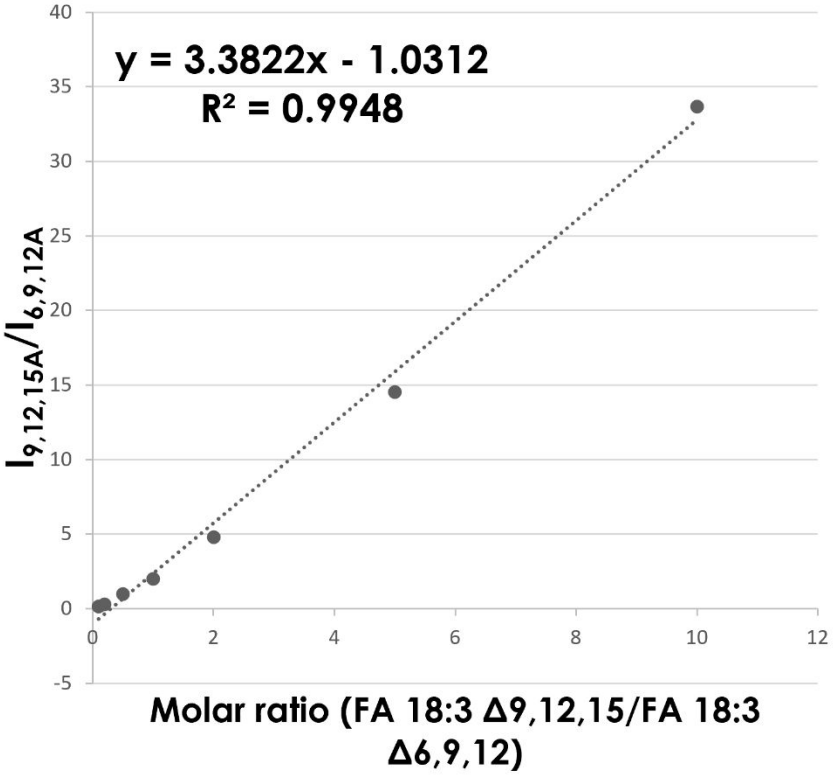

Figure S9. Linear relationship between the molar ratios of FA 18:3 Δ9,12,15 and Δ6,9,12 and the intensities of the diagnostic F_A ions ($I_{9,12,15A}/I_{6,9,12A}$).

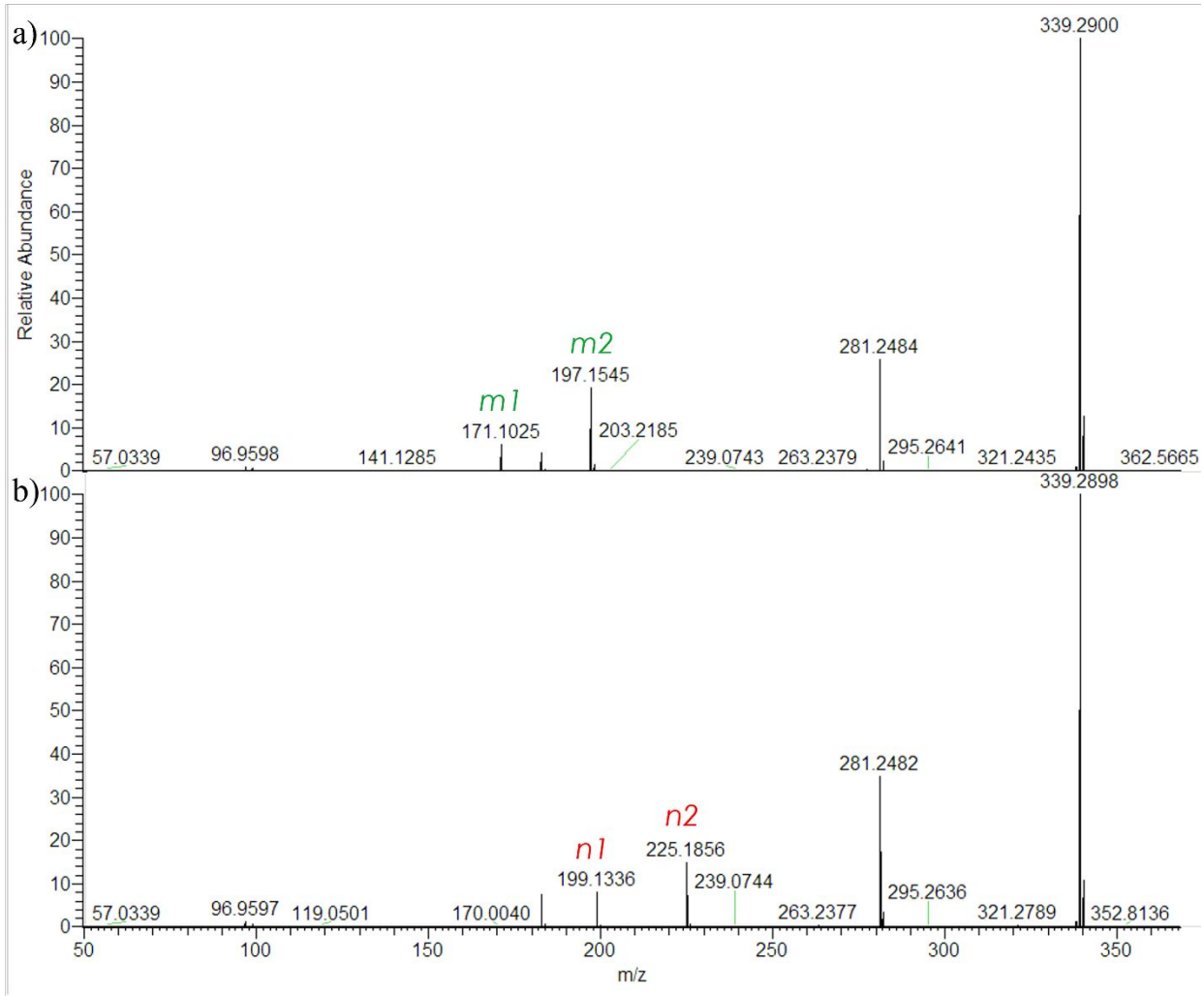

Figure S10. ESI(−)-HCD MS/MS spectrum (40 NCE) of (a) deprotonated FA 18:1 Δ9 and (b) deprotonated FA 18:1 Δ11 after PB derivatization with acetone. The reported nomenclature of the product ions is that of Ma (https://doi.org/10.1073/pnas.1523356113), with the two ions deriving from each of the two main PB products.

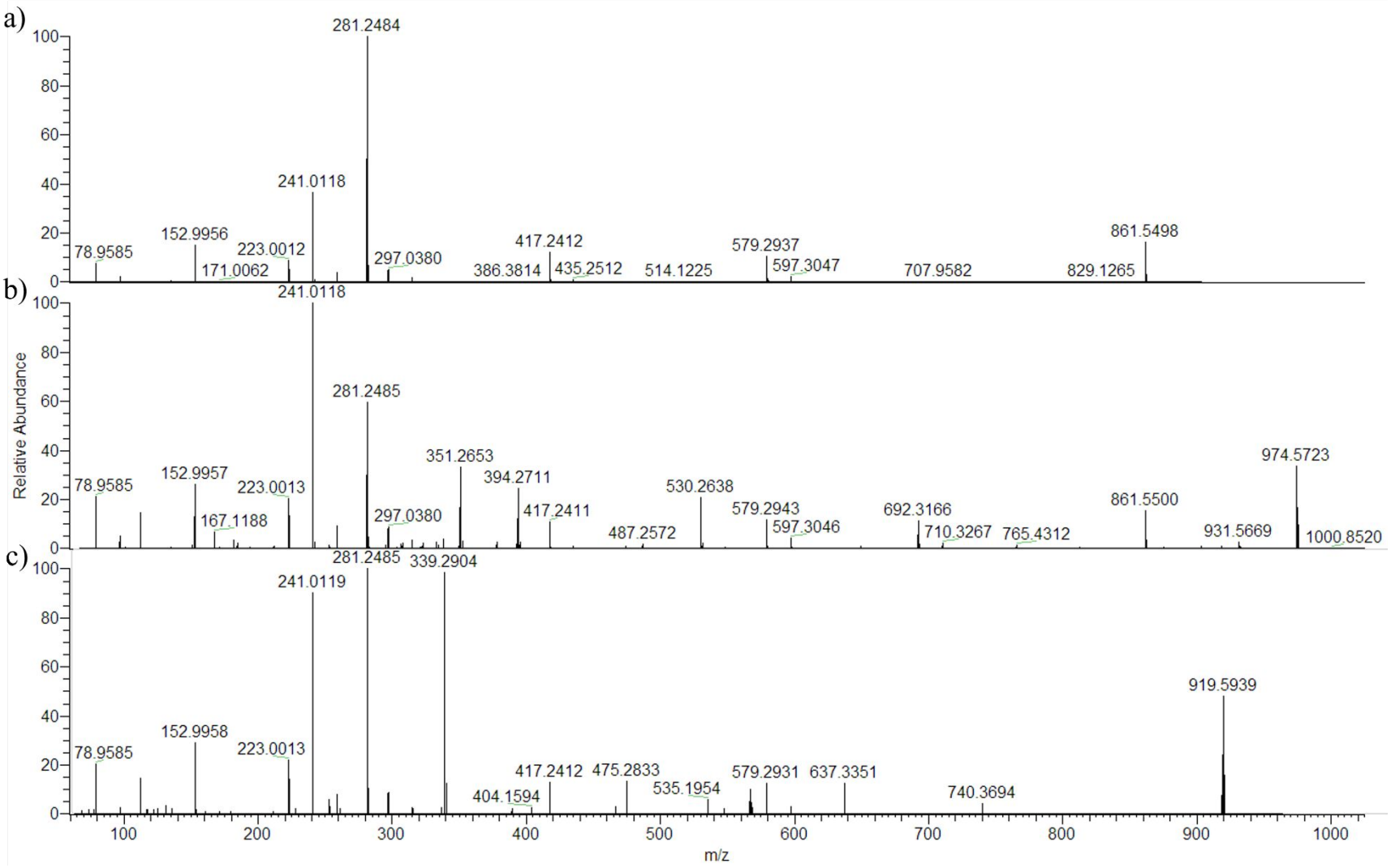

Figure S11. ESI(–)-HCD MS/MS spectrum (30 NCE) of a) underivatized PI (18:1/18:1); b) aPB derivative of PI (18:1/18:1); c) PB derivative of PI (18:1/18:1).

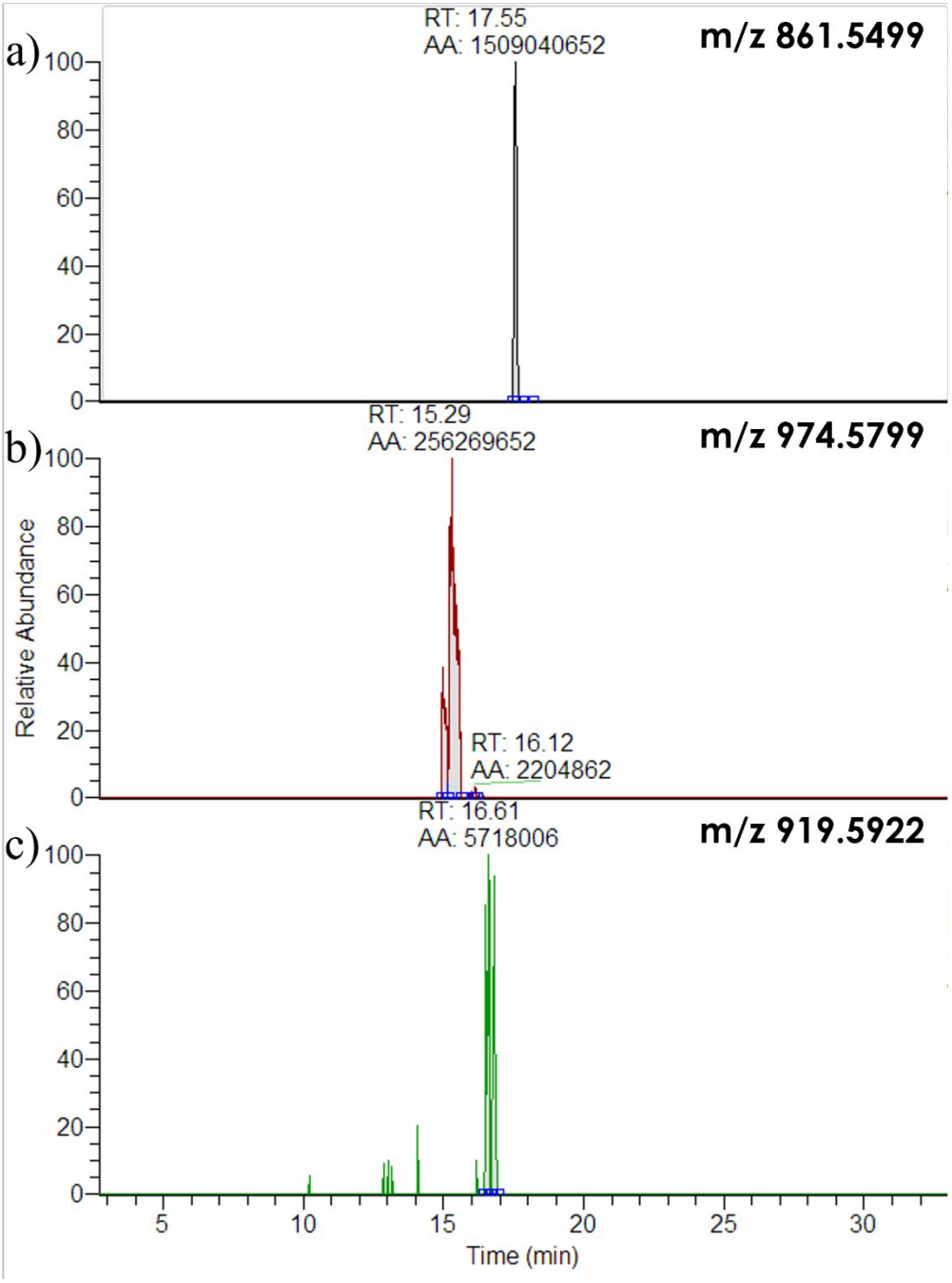

Figure S12. Total ion current of a) deprotonated underivatized PI (18:1/18:1); b) deprotonated aPB derivative of PI (18:1/18:1); c) deprotonated PB derivative of PI (18:1/18:1) obtained by the competitive aPB/PB reaction.

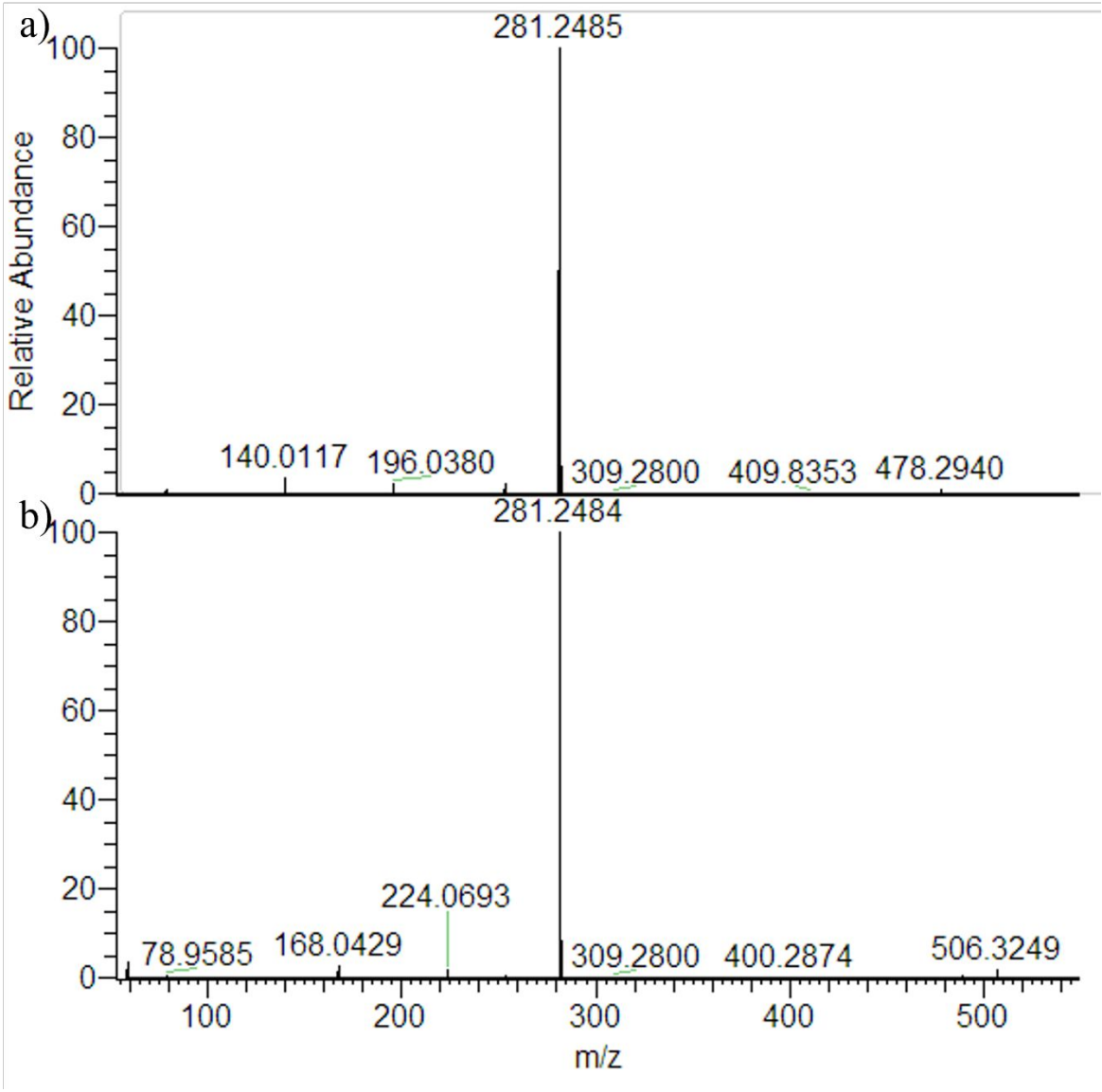

Figure S13. ESI(–)-HCD MS/MS spectrum (30 NCE) in negative ion mode of a) underivatized deprotonated PE (18:1/18:1); b) underivatized acetate adduct of PC (18:1/18:1).

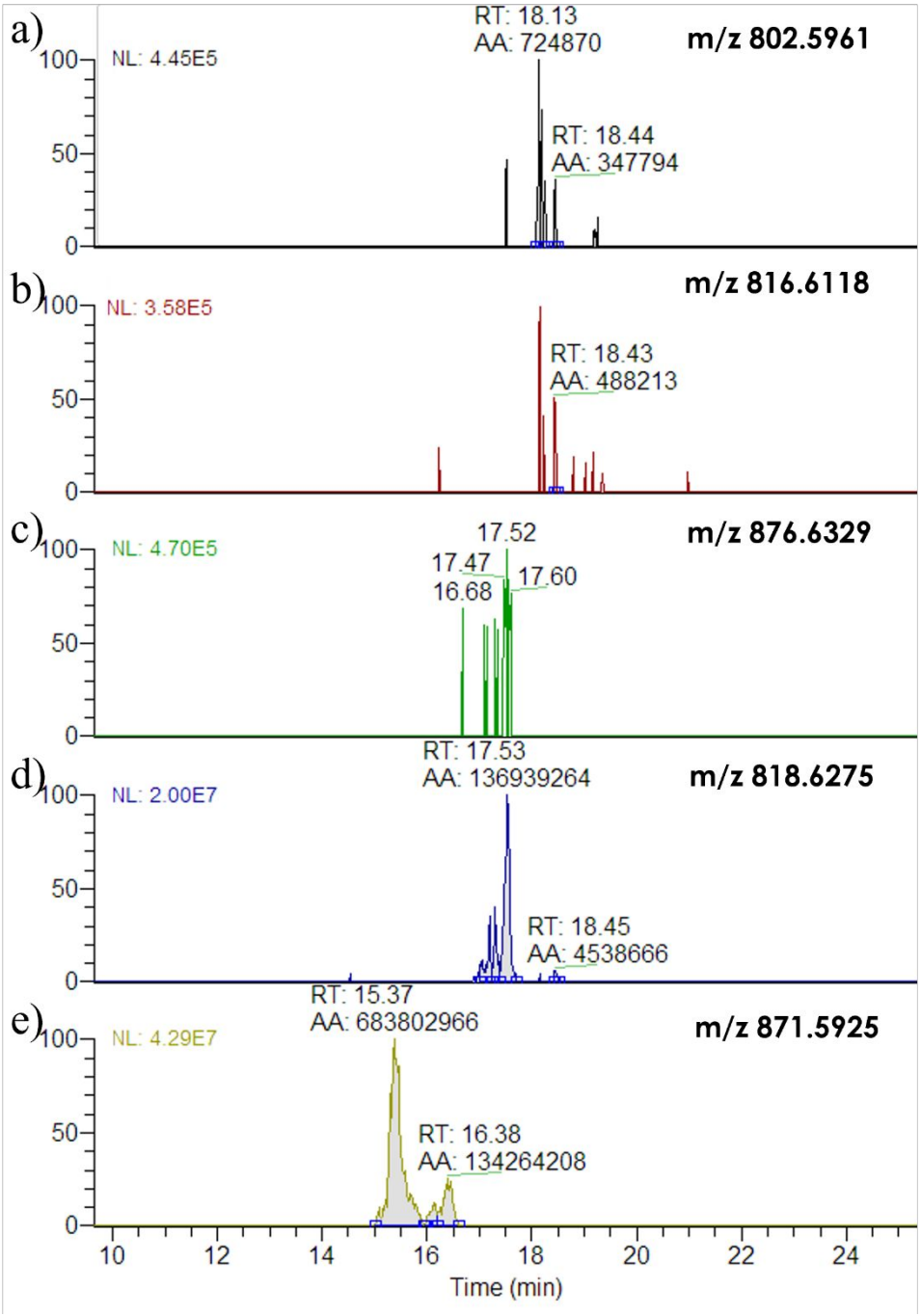

Figure S14. Total ion current of the m/z corresponding to a) the deprotonated PB derivative of PC (16:0/18:1); b) the demethylated PB derivative of PC (16:0/18:1); c) acetate adduct of the PB derivative of PC (16:0/18:1); d) the protonated PB derivative of PC (16:0/18:1); e) the deprotonated aPB derivative of PC (16:0/18:1).

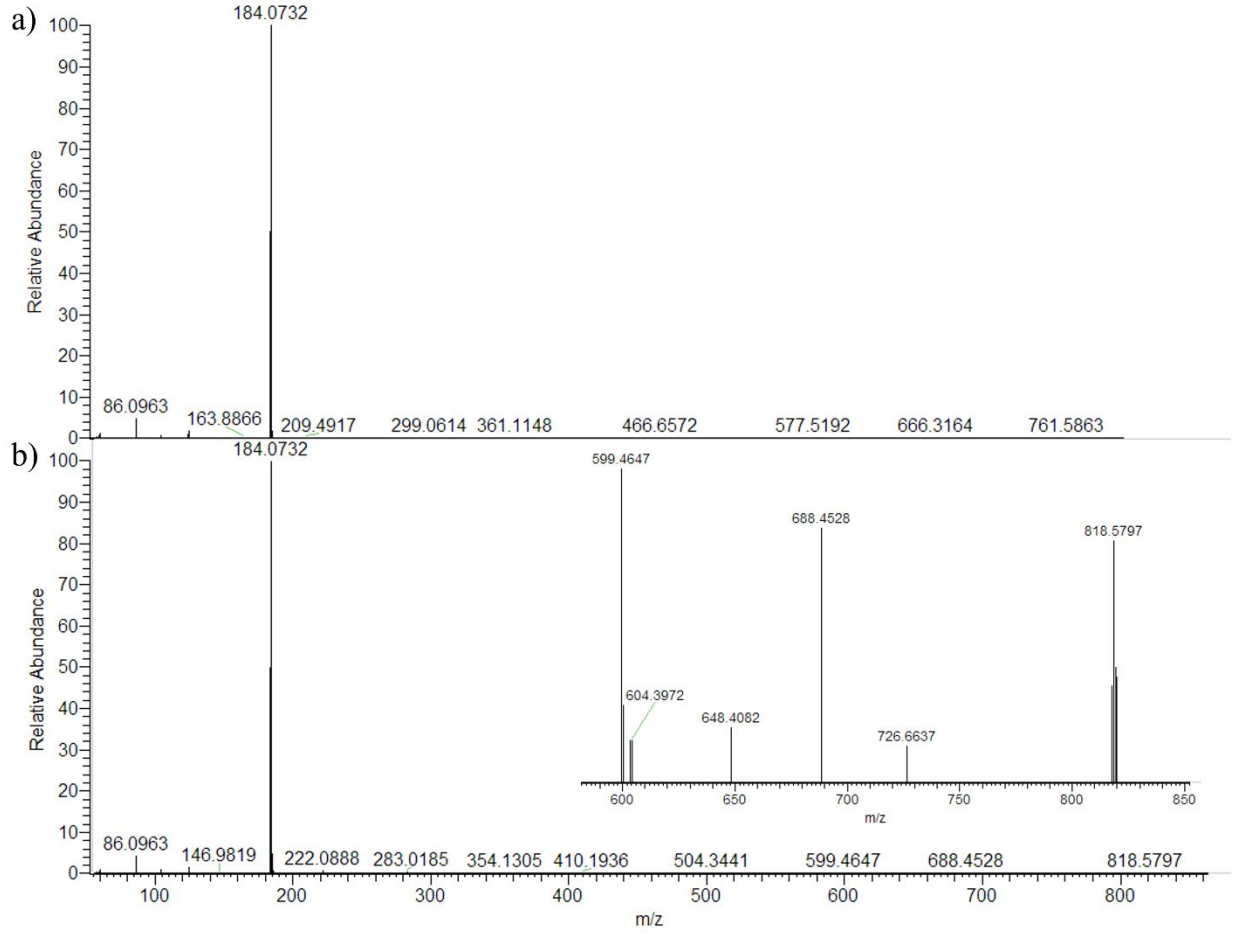

Figure S15. ESI(+)-HCD MS/MS spectrum (30 NCE) of (a) protonated underivatized PC (16:0/18:1) and (b) protonated PB-derivatized PC (16:0/18:1).

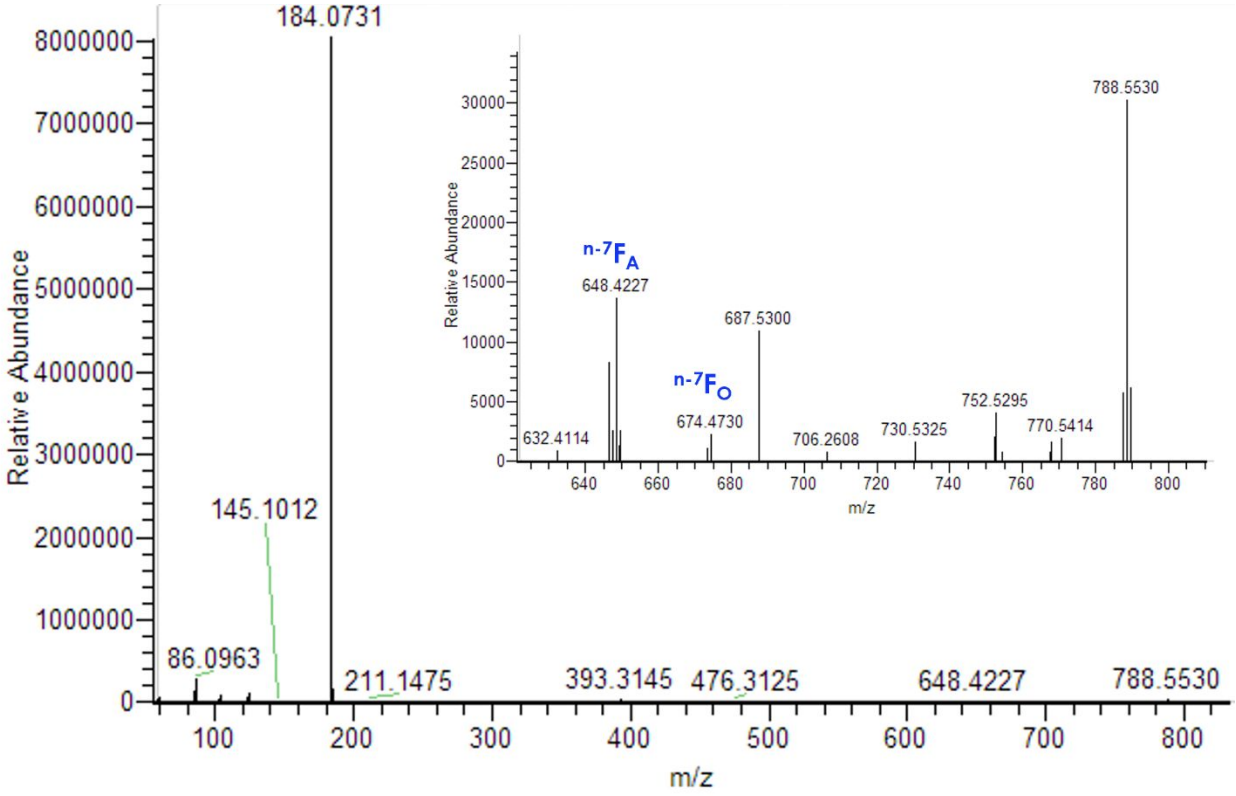

Figure S16. ESI(+)-HCD MS/MS spectrum (30 NCE) of protonated PB-derivatized PC (16:1/16:1) from the yeast extract. A zoom on the high m/z range shows a low abundance of the typical diagnostic peaks for pinpointing carbon-carbon double bonds.

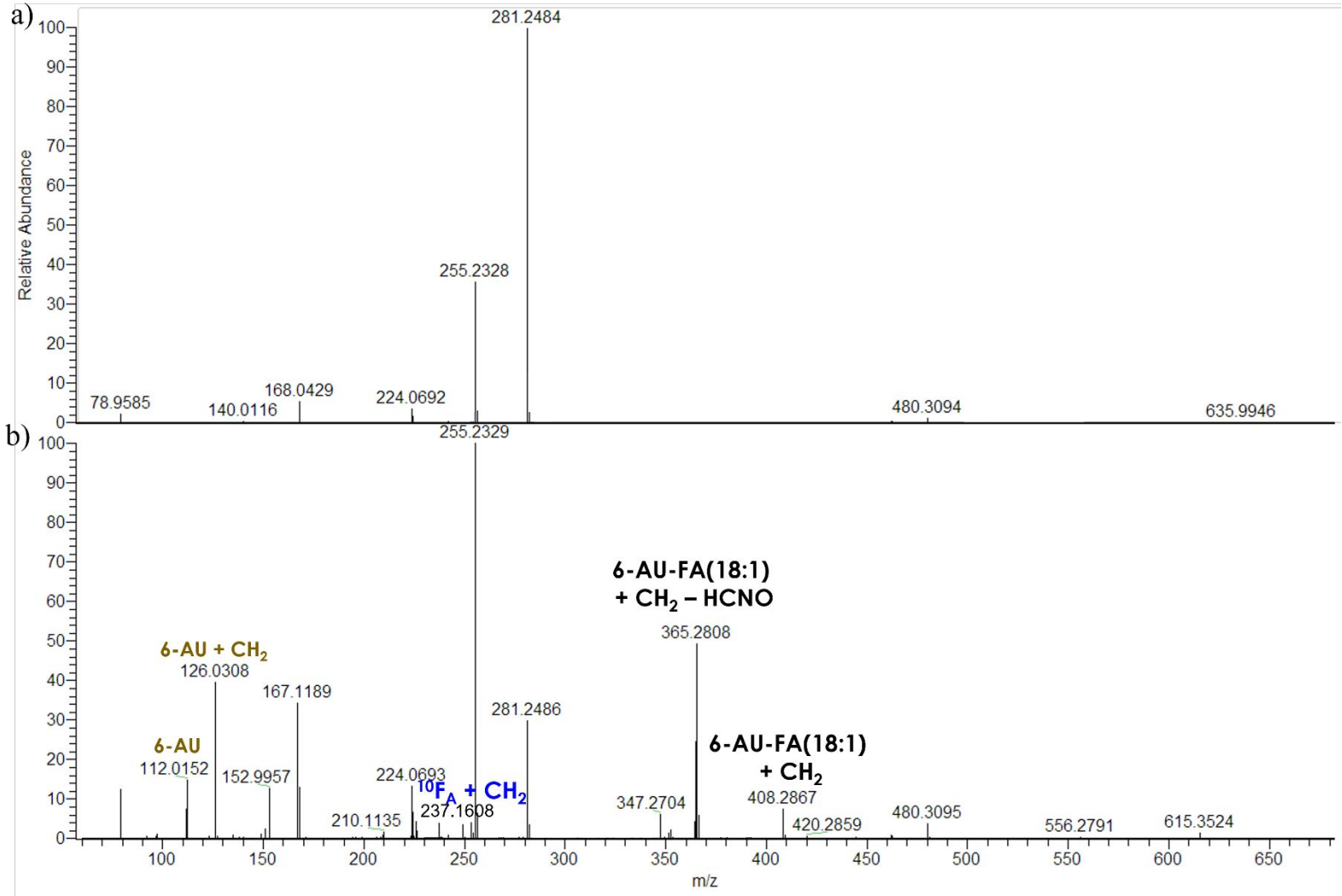

Figure S17. ESI(−)-HCD MS/MS spectrum (30 NCE) in negative ion mode of a) underivatized acetate adduct of standard PC (16:0/18:1); b) deprotonated aPB derivative of standard PC (16:0/18:1).

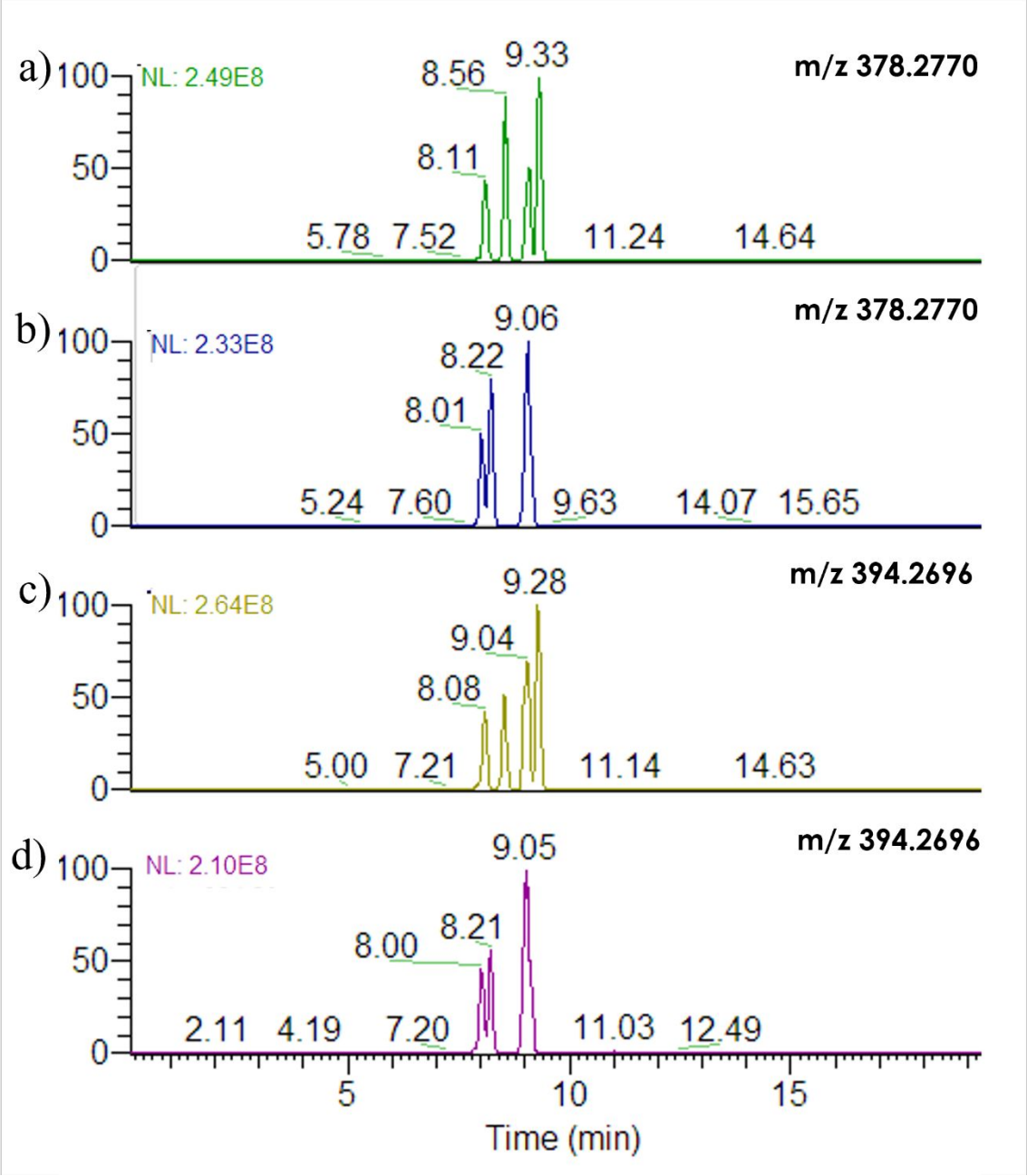

Figure S18. Total ion current of the m/z corresponding to a) the protonated in-source fragment of the aPB derivative of FA 18:1 Δ9; b) the protonated in-source fragment of the aPB derivative of FA 18:1 Δ11; c) the deprotonated aPB derivative of FA 18:1 Δ9; d) the deprotonated aPB derivative of FA 18:1 Δ11.

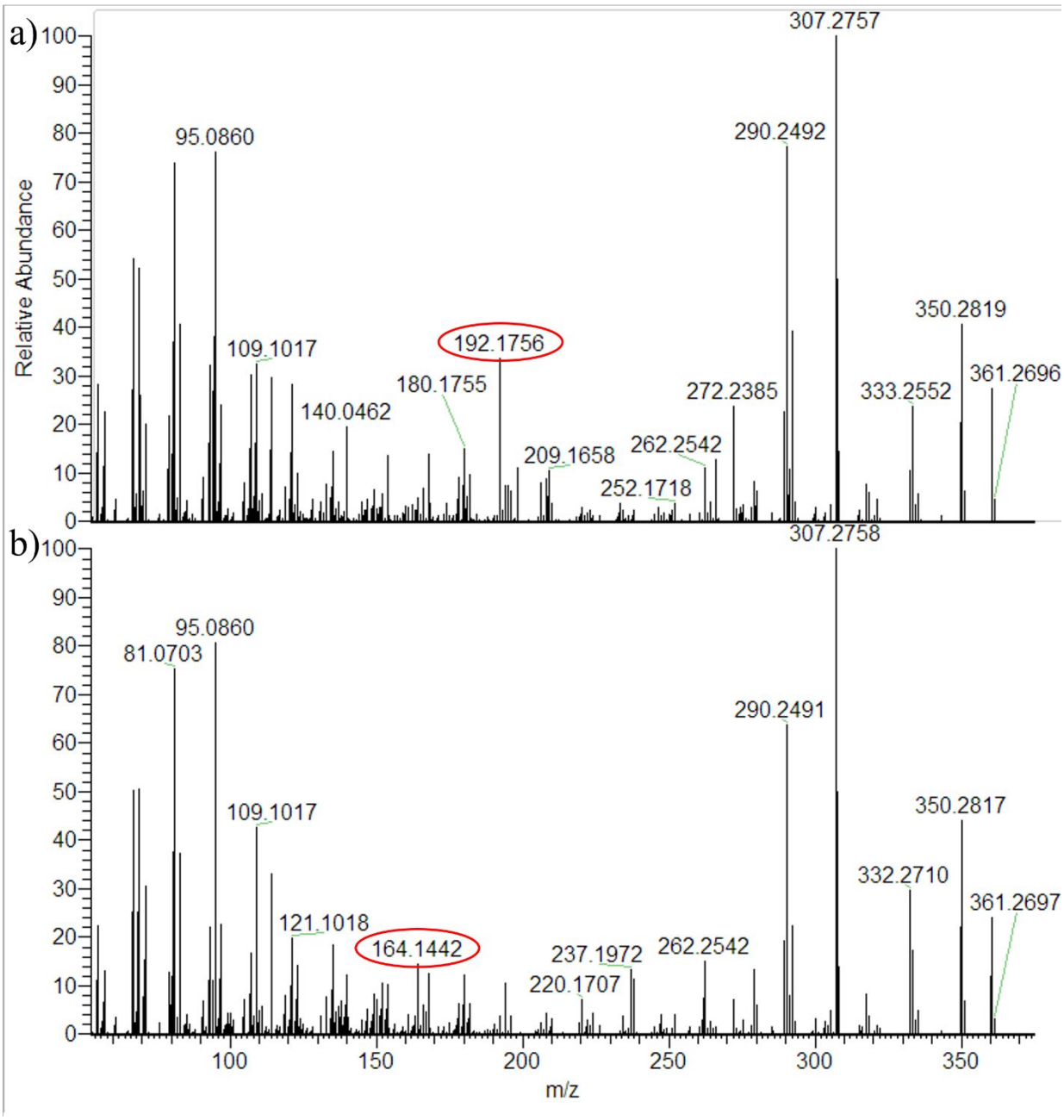

Figure S19. ESI(+)-HCD MS/MS spectrum (30 NCE) of a) the protonated aPB derivative of FA 18:1 Δ9; b) the protonated aPB derivative of FA 18:1 Δ11. The diagnostic ions are marked with a red circle. The relatively high HCD energy employed could explain the obtention of several ions from secondary processes in the low m/z range.

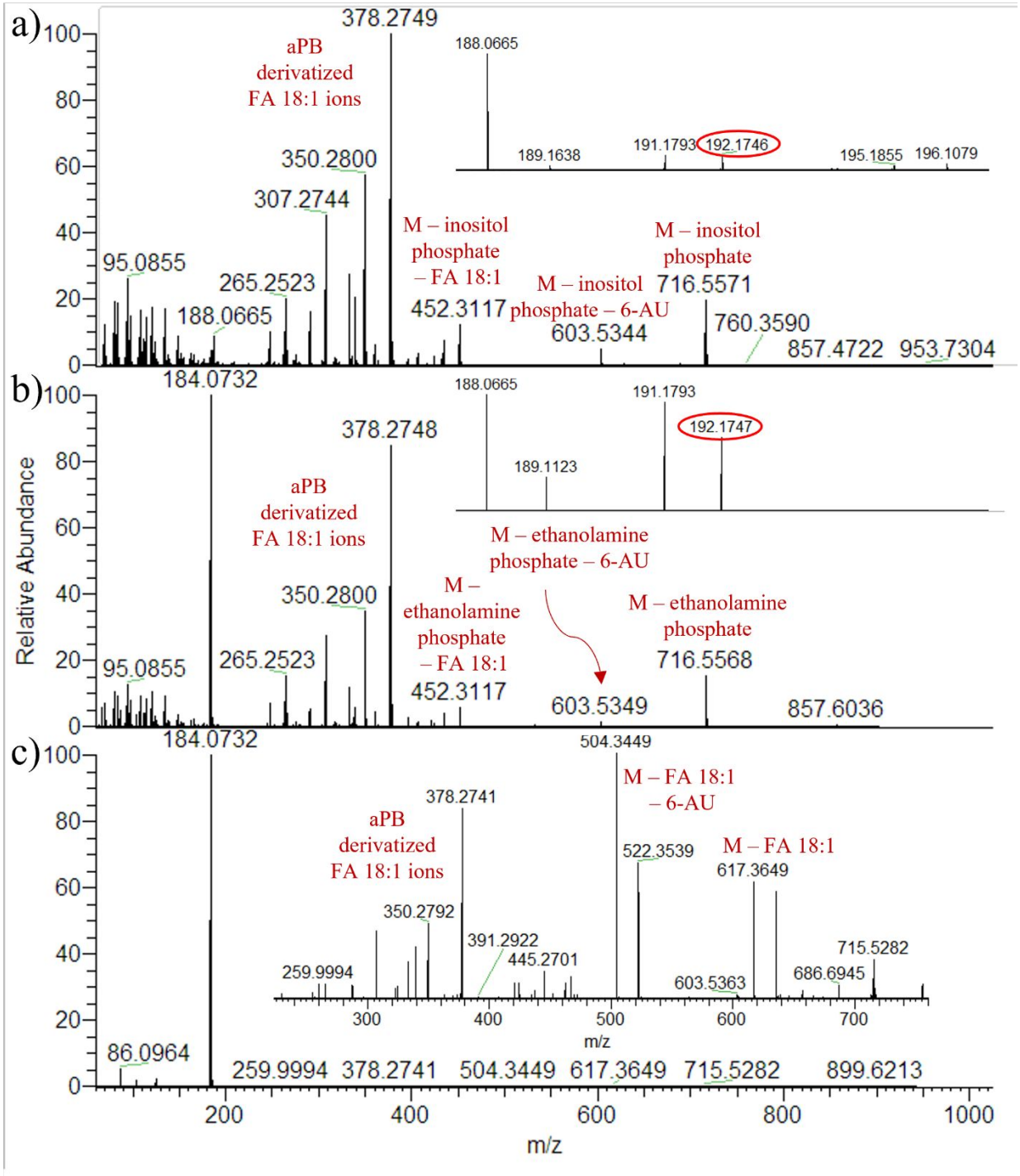

Figure S20. ESI(+)-HCD MS/MS spectrum (30 NCE) of a) the protonated aPB derivative of standard PI (18:1 Δ9/18:1 Δ9); b) the protonated aPB derivative of PE (18:1/18:1); c) the protonated aPB derivative of PC (18:1/18:1). The diagnostic ions are marked with a red circle. The

relatively high HCD energy employed could explain the obtention of several ions from secondary processes in the low m/z range.